Simulation and Validation of Bulk Micromachined 6H-SiC High-g Piezoresistive Accelerometer

Andrew R. Atwell[1], Robert S. Okojie[2], Kevin T. Kornegay[1], Scott. L. Roberson[3] and Alain Beliveau[4]

1Cornell University, School of Electrical and Computer Engineering, Ithaca, NY 14853
Ph: (607) 255-1418; Fax: (607) 254-4565; E-mail: ara7@cornell.edu
[2]NASA Glenn Research Center, 21000 Brookpark Road, MS 77-1, Cleveland OH 44135
[3]Air Force Research Laboratory, Munitions Directorate, AFRL/MNMF, Fuzes Branch, Eglin AFB, FL 32542
[4]Applied Research Associates, 2004 Lewis Turner Blvd., Union Station Suite C, Fort Walton Beach, Fl 32547

ABSTRACT

We report the utilization of key design parameters to simulate, batch-fabricate and evaluate first-generation single crystal 6H-SiC piezoresistive accelerometers for extreme impact, high electromagnetic fields (EM) and high temperature applications. The results from finite element analysis (FEA) of the selected design models were compared to evaluated prototypes. While FEA results predicted safe operation above 100,000-g's, preliminary experimental tests were performed up to 40,000-g's. Sensitivities ranging between 50 and 343 nV/g were measured. Non-linear behavior was observed over the shock range relative to the commercial accelerometer used as a benchmark. These initial results offer promise for the use of 6H-SiC accelerometers for extreme impact sensing in strong EM fields and temperature up to 600 ^{o}C that are beyond the capability of silicon.

INTRODUCTION

The need for improved system performance in extreme impact (>100,000-g's), high electromagnetic (EM) fields (> 18 Tesla in some railguns), and high temperature (>500 ^{o}C) environments has placed strong demand for more robust instrumentation. Commercially available accelerometers based on silicon technology have been demonstrated to survive nearly 100,000-g's [1], but its material properties may inhibit reliable operation in application-desired high temperatures (>350 ^{o}C) unless more complex and expensive packaging schemes are adopted [2]. In addition, these accelerometers must survive the EM fields associated with the all-electric vehicle technology for military and space applications. In response to these needs, a collaborative effort between the National Aeronautics and Space Administration (NASA) Glenn Research Center, the United States Air Force Research Laboratory (AFRL) Munitions Directorate, and Cornell University has initiated work aimed at establishing the critical enabling technology infrastructure (modeling, fabrication, and validation) required for the implementation of SiC accelerometers designed specifically for extreme environments. The choice of SiC is largely due to its excellent thermomechanical properties over silicon. Although with a relatively lower gauge factor of 30 [3] compared to silicon of about 90 [4], SiC compensates with a higher Young's modulus of approximately 448 GPa [5] compared to 129.5 GPa for (100) silicon [6]. SiC does not suffer from thermally induced plastic deformation associated with similarly designed silicon membranes when heated above 500^{o}C [7]. SiC has a melting temperature of around 2800 ^{o}C, compared to 1412 ^{o}C for silicon. In addition to its superior thermomechanical properties, single crystal SiC has a wide band gap ranging from 2.39 eV for the cubic 3C-SiC polytype to 3.2 eV for the 4H-SiC hexagonal polytype, compared to 1.12 eV for single crystal silicon. Therefore, thermal generation of carriers that results in increased reverse leakage current across the pn-junction is very minimal even at 600^{o}C.

In this initial effort, we have selected four different configurations within a design matrix and performed extensive micromechanical finite element analysis (FEA) [8] that included static, modal, and transient analyses. This was

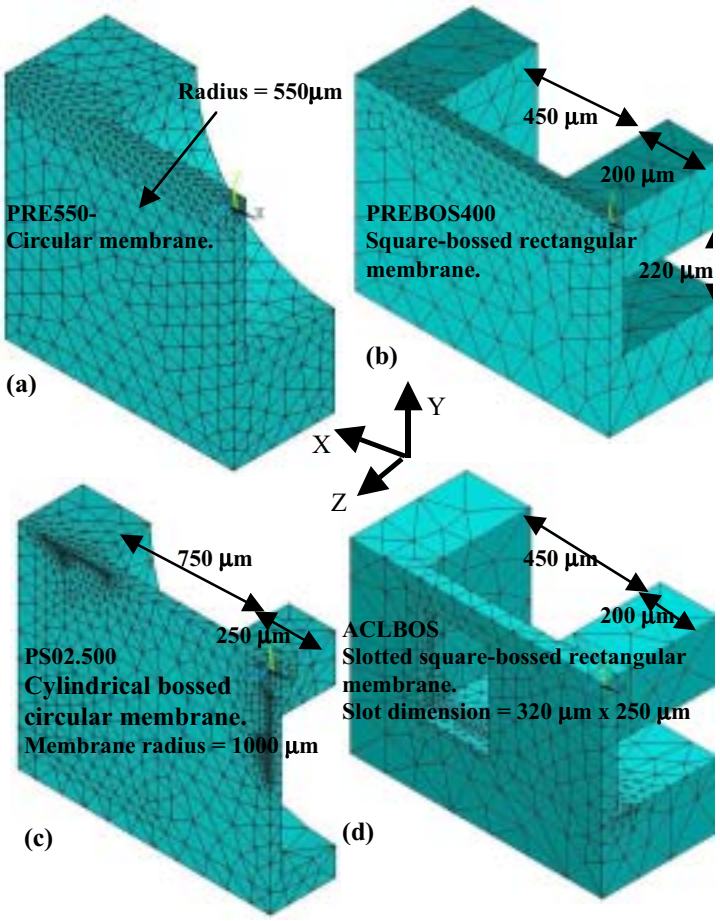

Figure 1: *Mesh of quarter-symmetry model for the four 6H-SiC device configurations analyzed and tested. Membrane thickness = 60 µm.*

followed by sensor fabrication and evaluation. For packaging, the sensors were epoxied into a ceramic dual-inline-pin package and aluminum wirebond was applied between the sensor and package. This un-optimized packaging used in the aggressive test environment was expected to cause significant deviation between FEA prediction and physical results. However, the interest at this initial study was to validate device survivability and worse case measurement deviation from a selected commercial-off-the-shelf accelerometer that was used as a benchmark [9]. The four designs investigated at this initial phase are described by the quarter-symmetry geometries shown in Figure 1. The PRE550 is a simple circular pressure membrane with a radius of 550 µm; the PREBOS400 is a square-bossed rectangular membrane with a 400 µm boss sides. The distance between the boss edge and the inner peripheral edge along the y-axis is 220 µm while in the x-direction it is 450 µm. The ACLBOS400 has the same dimension as the PREBOS, except for the rectangular slot in each quadrant to reduce damping and increase the sensitivity of the device. The dimension of each slot is 320 x 250 µm. The PS02.500 is a bossed circular membrane with boss edge to inner peripheral edge distance of 750 µm; and boss radius of 250 µm. The membrane thickness in all cases was approximately to 60 µm. To the best of our knowledge, this is the first reported demonstration of 6H-SiC accelerometers for high g applications.

ACCELEROMETER DESCRIPTION

The as fabricated 6H-SiC accelerometer chip sizes ranged from 4 mm^2 to 6.25 mm^2 in area, with Wheatstone bridge configured circuit. The piezoresistive mesa elements were dry-etched in (0001)-oriented n-type (doping level 3.8 x 10^{18} cm^{-3}) 6H-SiC epilayer grown by chemical vapor deposition on a high resistivity (7 Ω-cm) p-type 6H-SiC substrate. The scanning electron microscope of a representative ACLBOS400 configuration is shown in Figure 2a while a cross-section is shown in Figure 2b to depict the relative positions of the resistors. The four sensing elements are placed longitudinally on the narrow beams, each located on the inner edge of the peripheral rigid structure and at the opposite edges of the centered inertial proof mass (boss). Both the front side and backside were fabricated by a deep reactive ion etching process. The two narrow beams that carry the piezoresistors transfer strain to the piezoresistors, thereby effecting a change in output voltage of the Wheatstone bridge. The wider beams can be modified during design to predetermine the strain transferred to the narrow resistor-carrying beams. The two inner piezoresistors are placed on the center boss, but because of their length, they overhang the boss edge on two sides. Ideally, such placement allows both resistors to experience similar stress, compressive or tensile, depending on the direction of the applied external stimulus. Sections of the outer piezoresistors on the narrow structural beam also overhang the inner peripheral edge of the solid section as indicated in Figure 2b. When an external stimulus is applied, the stress component of these external resistors is, ideally, equal and have the same sign, but opposite that of the inner resistors.

The design considerations for the accelerometer take into account key design parameters that are required to develop robust SiC sensors to survive extreme environments. The key design parameters considered included the safe

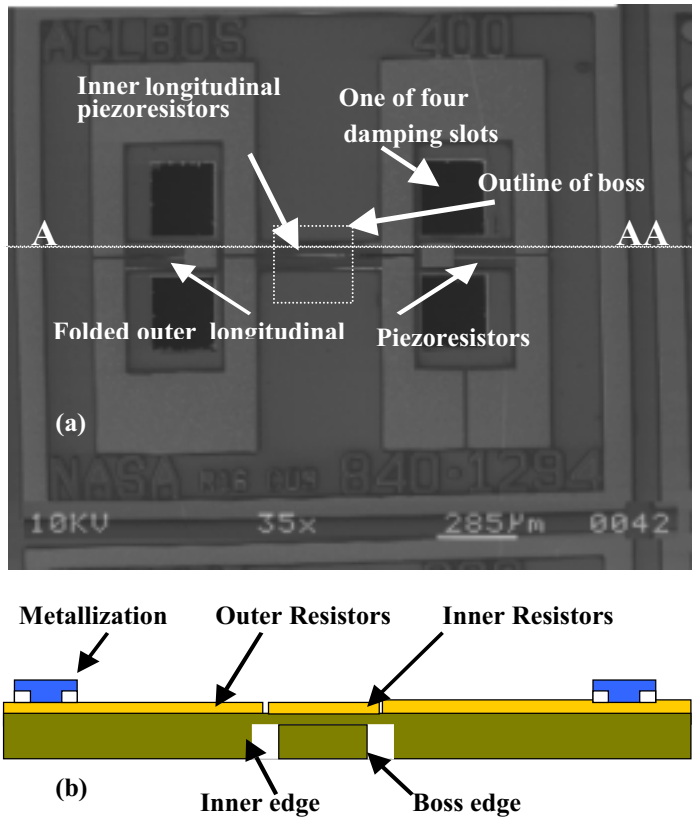

Figure 2: *a) SEM micrograph of accelerometer depicts the four longitudinal piezoresistors placed on the narrow beams; b) A-AA cross section of Figure 2a depicts the relative locations of the inner and outer resistors on the narrow beams*

operating stress (SOS), which took into consideration the inertial mass, diaphragm thickness and radius, and damping characteristics of the accelerometer design. In this work the maximum SOS was set at 50% of the fracture strength of SiC (450MPa) [10].

FINITE ELEMENT ANALYSIS

Simulations were performed to extract the behavioral parameters of the structure representing each design configuration. The FEA can analyze the distributed nature of the mass of the structure instead of the lumped mass approximation of the theory. The device geometry was either imported from the layout tool [11] or directly generated in the simulation tool where the solid geometry was cut into quarters and all but one quarter was deleted as depicted in Figure 1 to greatly reduced the analysis time. The element selected to mesh the solid geometry was SOLID187 [8] which is a higher order 3-D, 10-node element with quadratic displacement behavior and three degrees of freedom at each node: translations in the nodal x, y, and z directions. The boundary conditions were applied such that the back face (not

including the boss) was fixed in all three degrees of freedom to prevent rigid body motion. Then the symmetry boundary condition was applied to the exposed quarter-symmetry faces.

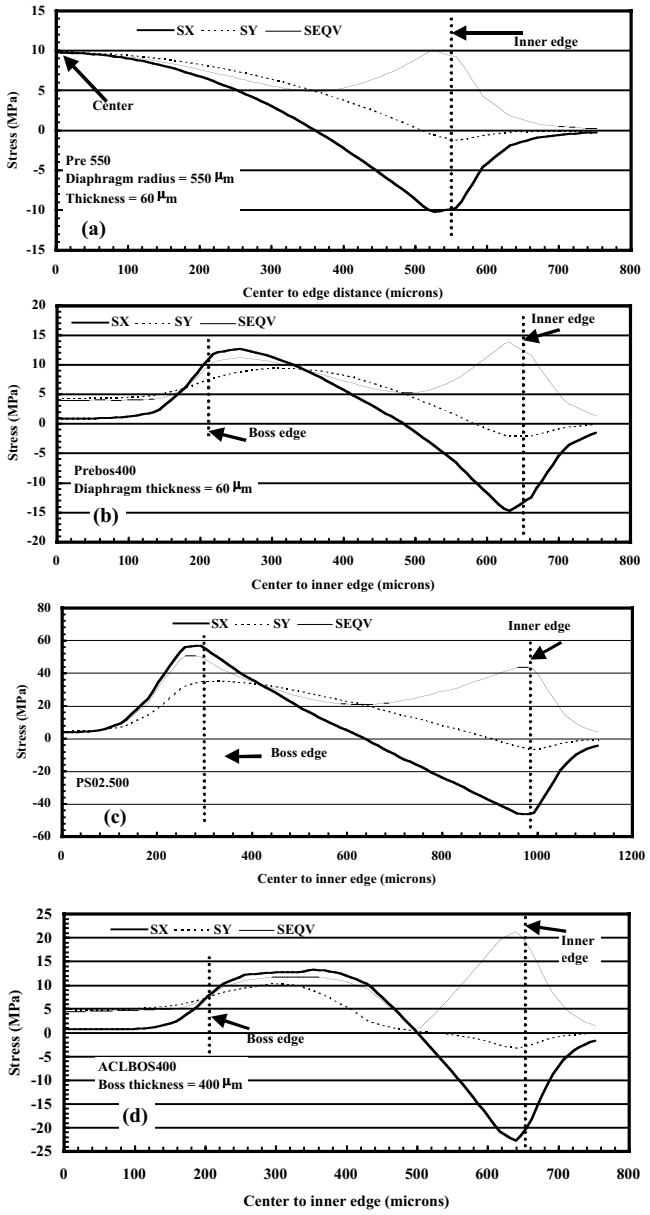

***Figure 3**: Static stress distribution along the x- and y-stress of the four 6H-SiC accelerometers show points of maximum tensile and compressive stress magnitudes at applied load of 100,000-g's. Note: The y-stress values are those intersecting the x-axis*

The stresses in the x- (SX) and y- (SY) directions and the von Mises equivalent stress (SEQV) are shown in Figures 3 a-d for an applied acceleration of 100,000-g's. The x-axis in each plot represents the distance along the A-AA line of Figure 2a, starting from the center and moving along that line to the right edge of each structure. This is the path along which the piezoresistors are located. The stress profile of PRE550 in Figure 3a follows the usual profile for a simple circular plate that is fixed at the edge. The stress in the x-direction is compressive at the edge and becomes tensile at the center and is approximately equal in magnitude as was found in [12]. Resistors placed at these locations will experience the highest sensitivity. Since both the x- and y-axis are essentially radial and tangential on circular diaphragms, the resistors at the center location will experience large tangential Poisson strain that adds negative piezoresistance parasitic to the measured output. In Figure 3b (PREBOS400), the maximum stress in the compressive and tensile regions is not equal. This implies unequal sensitivity between the inner and outer resistors. However, the y-axis stress component is reduced, thereby minimizing the parasitic. In Figure 3c, which has a cylindrical boss, the x-axis stress at both regions is also opposite in signs and unequal in magnitude. In this case too, the y-axis stress at the boss edge is relatively less than its corresponding x-axis stress at the same section, but the resistors will also experience unequal sensitivity. The stress profile in Figure 3d (ACLBOS400) is similar to PREBOS. Also, like PREBOS, the magnitudes of the stresses in the tensile and compressive regions are not equal. However, the stress is relatively higher at the outer edge than the PREBOS400, indicating the effect of having perforations in the diaphragm. The observed asymmetry in the stress magnitudes at the inner and outer resistors for the bossed structures is an area where geometric optimization will be needed.

A compilation of results from the FEA is presented in Table 1 for the following: maximum displacement in the z-direction, the stresses at regions where the resistors were placed, and the first natural frequency mode, f_1. The applied load of 100,000-g's is the same for all cases. The radii or length between boss edge and inner edge are shown in Figures 3 a-d. It can be seen that except for the PRE550, the maximum compressive and tensile stress magnitudes in other configurations are unequal. In all cases, however, the maximum stress magnitude is less than 50 % of the fracture strength of SiC of 450 MPa. The first frequency mode, f_1, is

Device	Z-(μm)	SX outer edge (MPa)	SX boss edge (MPa)	$SEQV_{max}$ (MPa)	f_1 (kHz)
PRE550	0.05	-9.89	9.74	15	875
PREBOS400	0.06	-13.6	9.25	37	657
PS02.500	0.47	-40.8	52.8	82	253
ACLBOS400	0.07	-21.6	7.15	147	621

***Table 1:** Comparison of values for the four accelerometer configurations at 100,000-g's.*

higher than 600 kHz in all cases except the PS02.500. This is expected, since the active section of this structure is larger than the others. It also explains why PRE550 with a smaller active radius of 550 μm has the highest f_1 of 875 kHz. This is crucial for high-g impacts since such event releases spurious high frequencies. Therefore, devices such as PS02.500 with lower f_1 of 253 kHz will be susceptible to lower frequency vibratory modes that will create instability in the device performance. This is an example of trading-off performance, i.e., in low natural frequency for high sensitivity.

ACCELEROMETER EVALUATION

The evaluation of the SiC accelerometers was conducted on a very high-g machine (VHG), which is a pneumatically driven shock evaluation instrument used to produce a short duration, high frequency impact response. The Navy Ordinance Laboratory developed this apparatus and the detailed characteristics of its components are reported in a Naval Ordinance Laboratory Report [13]. It operates by applying a predetermined pressure for a specific g level to the low-pressure air chamber. When the specified pressure is reached, a lever is activated which causes a 30 lb. piston to accelerate and impact the steel anvil, which is held in place by an aluminum fixture. This anvil provides a mounting surface for the devices to be evaluated. The acceleration imparted to the test item is dependent upon the impact velocity of the piston, as well as the masses of the test item, the test fixture, the test cartridge, and the piston. The VHG machine was designed to perform impact evaluations to 100,000 g's.

The reference accelerometer that was chosen for this investigation was an ENDEVCO 7270-60K with a sensitivity of 3 +2/-1.5 μV/g [9]. This accelerometer is etched from a single piece of silicon to create the sensing system. It has a high resonant frequency along with low impedance, high over-range, and zero overdamping, which allows for no phase shift.

The first SiC MEMS device evaluated was the PREBOS400, the rectangular boss design. As shown in Figure 4, the device (in gray) reasonably replicated the output

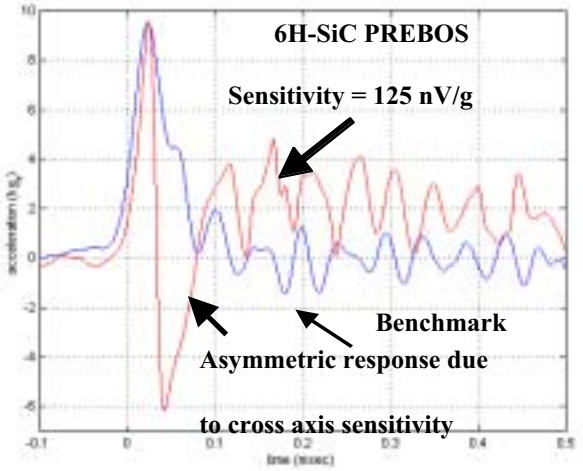

Figure 4: *Acceleration output plot of the benchmark and 6H-SiC MEMS square-bossed rectangular diaphragm design at 9,000-g's. The SiC MEMS has a rapid reversal of the signal around 0.05 msec.*

of the benchmark (in black) for the first acceleration peak until a rapid reversal of the signal was encountered around 0.05 msec. The reversal of the signal was not encountered until the shock test levels reached 8,000-g's and below this value the SiC MEMS device matched the benchmark output in frequency and magnitude for the shock pulse. Above 8,000-g shock levels, the reversal of the signal became more rapid and as the shock level was increased the measured shock level by the SiC MEMS device decreased. This phenomenon of the signal output above 8,000-g's can be attributed to two possible causes: (1) The device membrane and boss impact a mechanical stop on the chip and reversed direction, and/or (2) The device has asymmetric dynamic behavior between the wide and narrow beams. Either or both

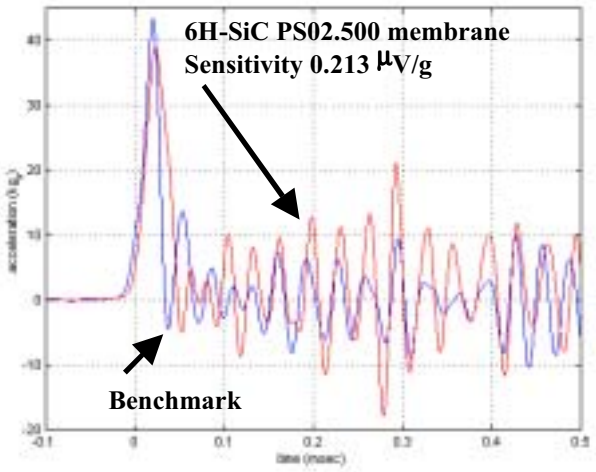

Figure 5: *Acceleration output plots of the benchmark and 6H-SiC bossed circular membrane design at 42,000-g's. The SiC MEMS matched the shape of the benchmark output but was nonlinear over the acceleration spectrum to 40,000-g's.*

of these could result in the above phenomenon of decreasing peak acceleration output with increasing shock levels. However, of these two possible causes, the latter seems more likely due to the recovery of the device around 0.1 msec with no apparent damage to the device.

As shown in Figures 5 and 6a, the output of the SiC devices with a bossed circular membrane (PS02.500) and simple circular (PRE550) membrane, respectively, indicate that the output shapes of the SiC devices (in gray) are very similar to the benchmark (in black). However, the PS02.500 device in Figure 5 does not match all the peak acceleration values in the evaluation series to 40,000-g's of the benchmark and thus is non-linear. This non-linearity is believed to be due to either a base strain in the device after fabrication or a slight misalignment of the piezoresistors on the diaphragm in a region of non-linear strain. We also observed that the non linearties in the configurations evaluated thus far appear to roughly coincide with the unevenness in the tensile and compressive stress magnitudes shown in Table 1.

The first peak response of the simple circular membrane 6H-SiC accelerometer (PRE550) in Figure 6a tracks the benchmark very well. This device has a smaller diameter and thus is stiffer and has a lower sensitivity (50 nV/g). The output of this device after the first peak varies greatly from the benchmark due to cable noise. The output signal of this device is four times less than the other 6H-SiC configurations tested and thus has a lower signal to noise ratio. In addition, this device was tested un-powered and similar outputs were observed with and without power after 1.3 msec. This has been observed in other devices (silicon commercial devices)

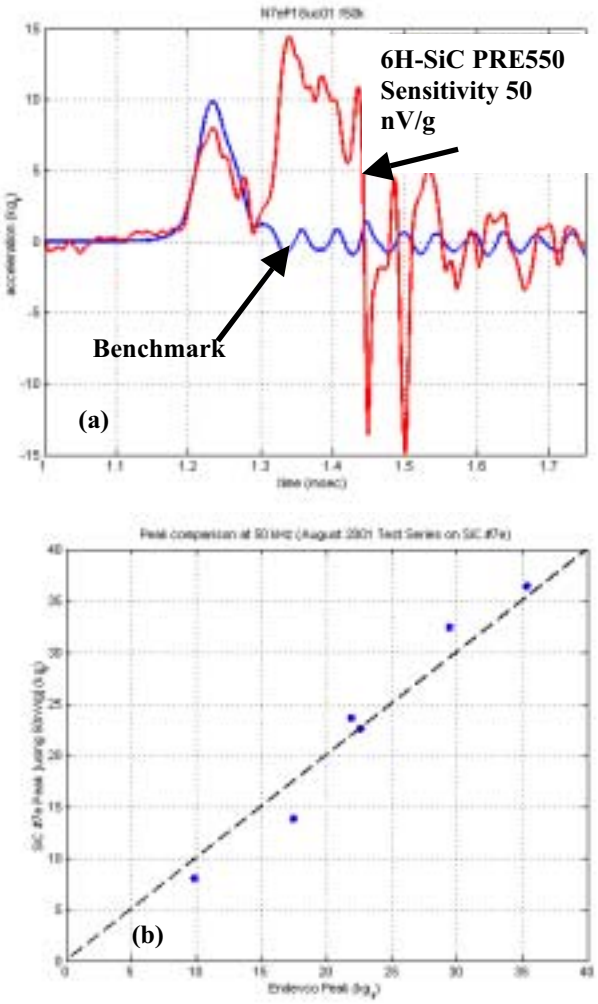

Figure 6: *Acceleration output plots of the benchmark and SiC round un-bossed membrane with smaller diameter at 10,000-g's. The SiC matched the shape of the benchmark output for the first shock pulse but did not match the output at lower frequencies due to cable noise. The first acceleration peak output was linear and matched to 40,000-g's.*

with sensitivities below 100 nV/g. However, the first peak acceleration data as shown in Figure 6b is linear and approximates the benchmark output up to 40,000-g's. An observation of Table 1 will show that the tensile and compressive stress magnitude of this configuration are practically equal and has the highest f_1 mode at 875 kHz.

CONCLUSION

Extreme impact instrumentation requires that sensing devices be stiff enough to survive and possess a high natural frequency to protect them against damage from spurious high frequency modes generated during impact. Our initial analysis and evaluations have determined that for piezoresistive based devices, the geometry will need to be optimized to combine stiffness for survivability and concentrated stress for improved sensitivity without necessarily trading off high natural frequency. We have also used key design parameters to demonstrate for the first time the feasibility of using 6H-SiC as a high-g piezoresistive accelerometer. Future work in this direction will involve design optimization that includes control of the damping characteristics, packaging, and high temperature characteristics.

ACKNOWLEDGEMENT

We wish to express our gratitude to NASA Glenn Research Center for funding this work under the 2000/2001 Internship Program (LERCIP) as well as Dan Segalman of the Air Force Office of Scientific Research (AFOSR) for supporting this effort. Author RSO thanks Drs. Phil Neudeck, Larry Matus, and Jih-Fen Lei at NASA Glenn Research Center for the critical reviews.

REFERENCES

[1] T. G. Brown, B. Davis, D. Hepner, J. Faust, C. Myers, C. Muller, T. Harkins, M. Holis, and B. Placzankis, "Strap-Down Microelectromechanical (MEMS) Sensors for High-G Munition Applications,"*IEEE Trans. on Magnetics*, vol: 37 No. 1, pp. 336-342, Jan. 2001.

[2] G. L. Katulka, D. J. Hepner, B. Davis, E. Irwin, M. Ridgley, and K. Kornegay, "Characterization of Silicon Carbide and Commercial-Off-The-Shelf (COTS) Components for High-g Launch and EM Applications," *IEEE Trans on Magnetics*, vol: 37 No.1, pp. 248-251, Jan. 2001.

[3] J. S. Shor, L. Bemis, and A. D. Kurtz, "Characterization of monolithic n-type 6H-SiC piezoresistive sensing elements," *IEEE Trans. Electron Devices*, vol. 41. pp. 661-665, May 1994.

[4] M. J. Madou, *The MEMS Handbook* ed. M. Gad-el-Hak, CRC Press, Boca Raton, Chapter 16, pp. 28, 2001.

[5] Silicon Carbide, eds. H. K. Henisch and R. Roy, Pergamon Press, New York, pp. 367, 1968.

[6] J. C. Greenwood, "Silicon in Mechanical Sensors," *J. Phys. E., Sci. Instrum.,* 21, pp. 1114-1128, 1988.

[7] A. D. Kurtz, T. A. Nunn, and R. A. Weber, US Patent # 4,672,354, 1987.

[8] ANSYS Inc. 201 Johnson Road, Houston, PA 15342-1300.

[9] Endevco Corporation, 30700 Rancho Viejo Road, San Juan Capistrano, CA 92675.

[10] E. Savrun and C. Toy, "An Aluminum Nitride Package for 600 °C and Beyond," Proceedings, 4th Intl. High Temperature Electronics Conf., Albuquerque, New Mexico, pp. 265-268, June 14-18, 1998.

[11] MEMSCAP Inc. 180 Grand Avenue, Oakland, CA 94612.

[12] S. Timoshenko and S. Woinowsky-Krieger, *Theory of Plates and Shells*, 2nd ed., McGraw-Hill, Inc., New York, pp. 56, 1959.

[13] V. F. DeVost, "Vhg Impact Test Set", Naval Ordnance Laboratory Technical Report, pp. 68-158, September 1968.